The Core Structure of X Generated in the Assembly of the Diiron Cluster of Ribonucleotide Reductase: $^{17}O_2$ and $H_2{}^{17}O$ ENDOR

Doug Burdi,[†] Jean-Paul Willems,[‡] Pam Riggs-Gelasco,[†] William E. Antholine,[§] JoAnne Stubbe,*[,†] and Brian M. Hoffman*[,‡]

Contribution from the Department of Chemistry, Massachusetts Institute of Technology, Cambridge, Massachusetts 02139-4307, Department of Chemistry, Northwestern University, Evanston, Illinois 60208-3113, and National Biomedical ESR Center, Medical College Wisconsin, Milwaukee, Wisconsin 53226

Received July 9, 1998. Revised Manuscript Received September 29, 1998

Abstract: The intermediate, designated **X**, formed during the self-assembly reaction of the tyrosyl radical/μ-oxo-bridged diferric cofactor in the R2 subunit of *Escherichia coli* ribonucleotide reductase (RNR) is directly involved in the oxidation of Y122 to the catalytically essential ·Y122. Earlier rapid freeze-quench (RFQ) Q-band ENDOR studies led to the formulation of **X** as a spin-coupled Fe^{III}/Fe^{IV} center, with an $S = {}^1/_2$ ground state, and showed that **X** contains a single terminal aqua ligand (water molecule or 2-fold disordered hydroxyl) bound to Fe^{III} but does not contain an hydroxyl bridge. That ENDOR data, coupled with RFQ-EXAFS data, plus the strong spin coupling between the iron ions constrain the structure of **X** to a di- or tribridged species whose inorganic core (defined as iron and exogenous ligands) contains the $[(H_xO)Fe^{III}OFe^{IV}]$ fragment. To determine whether the core contains a second oxo bridge and to establish the fate of the atoms derived from O_2, we have now performed CW *and* pulsed Q-band ^{17}O ENDOR experiments on samples of **X** prepared in both $H_2{}^{17}O$ and $^{17}O_2$, using a uniformly ^{15}N-labeled protein, [U-^{15}N]-R2. These measurements, along with kinetic studies on the formation of **X** in both wild-type and Y122F R2, as monitored by both ENDOR and S-band EPR spectroscopies, reveal that **X** contains two oxygen atoms. Both are initially derived from O_2, with one present as a μ-oxo bridge and one as the terminal aqua ligand; with time the latter of these atoms exchanges with solvent. These and our previous studies indicate that **X** does not contain a di-μ-oxo- or μ-oxo,hydroxo-bridged core structure. A structure for **X** is proposed that contains a single oxo bridge, one terminal aqua ligand bound to the Fe^{III}, and one or two additional mono-oxo bridges provided by the carboxylate oxygens of E115 and/or E238. In addition, the time course of the formation of **X** in the presence of $^{17}O_2$ provides important insights into the dynamics of cluster assembly.

Introduction

The self-assembly reaction of the tyrosyl radical/μ-oxo-bridged diferric cofactor in the R2 subunit of *Escherichia coli* ribonucleotide reductase (RNR) from its diferrous precursor and oxygen offers an opportunity to compare its chemical reactivity with those of a growing and increasingly diverse class of non-heme diferrous proteins,[1−3] including soluble methane monooxygenases (MMOH), fatty acid desaturases, alkane hydroxylases, and hemerythrin (Hr). The nitrogen-rich ligand environment of Hr[4−6] and alkane hydroxylases[7] contrasts with the carboxylate-rich environment of Δ^9-desaturase,[8] MMOH,[9] and RNR.[10,11] At present, the factors which govern the nature of dioxygen activation in these diverse systems remain unclear. The chemistry of MMOH and RNR has been most extensively studied to date.[2,3] Incubation of the diferrous form of MMOH with O_2 leads to the two-electron oxidation of methane to methanol, while reaction of diferrous-R2 with O_2 leads to the one-electron oxidation of tyrosine residue 122 (Y122) to the catalytically essential tyrosyl radical (·Y122). The intermediate observed in single turnover studies on MMOH, designated **Q**,[12−15] is proposed to be directly involved in the oxidation of methane. **Q** remains distinct from the intermediate, designated **X**, directly involved in the oxidation of Y122 to ·Y122 of R2.[16−18] One of the primary goals in the study of intermediates involved in these oxidations is to gain insight into how the ligand

[†] Massachusetts Institute of Technology.
[‡] Northwestern University.
[§] Medical College Wisconsin.

(1) Kurtz, D. M. *Chem. Rev.* **1990**, *90*, 585−606.
(2) Feig, A. L.; Lippard, S. J. *Chem. Rev.* **1994**, *94*, 759−805.
(3) Wallar, B. J.; Lipscomb, J. D. *Chem. Rev.* **1996**, *96*, 2625−2657.
(4) Shiemke, A. K.; Loehr, T. M.; Sanders-Loehr, J. *J. Am. Chem. Soc.* **1984**, *106*, 4951−4956.
(5) Stenkamp, R. E.; Sieker, L. C.; Jensen, L. H.; McCallum, J. D.; Sanders-Loehr, J. *Proc. Natl. Acad. Sci. U.S.A.* **1985**, *82*, 713−716.
(6) Shiemke, A. K.; Loehr, T. M.; Sanders-Loehr, J. *J. Am. Chem. Soc.* **1986**, *108*, 2437−2443.
(7) Fox, B. G. In *Comprehensive Biological Catalysis*; Sinnott, M., Ed.; Academic Press Ltd.: San Diego, CA, 1998; Vol. 3, No. 34, pp 261−348.
(8) Fox, B. G.; Shanklin, J.; Somerville, C.; Munck, E. *Proc. Natl. Acad. Sci. U.S.A.* **1993**, *90*, 2486-2490.
(9) Rosenzweig, A. C.; Nordlund, P.; Takahara, P. M.; Frederick, C. A.; Lippard, S. J. *Chem. Biol.* **1995**, *2*, 409−418.
(10) Nordlund, P.; Eklund, H. *J. Mol. Biol.* **1993**, *232*, 123−164.
(11) Logan, D. T.; Su, X. D.; Aberg, A.; Rengnstrom, K.; Hajdu, J.; Eklund, H.; Nordlund, P. *Structure* **1996**, *4*, 1053−1064.
(12) Liu, K. E.; Wang, D.; Huynh, B. H.; Edmondson, D. E.; Salifoglou, A.; Lippard, S. J. *J. Am. Chem. Soc.* **1994**, *116*, 7465−7466.
(13) Liu, K. E.; Valentine, A. M.; Qui, D.; Edmondson, D. E.; Appelman, E. I.; Spiro, T. G.; Lippard, S. J. *J. Am. Chem. Soc.* **1995**, *117*, 4997−4998.
(14) Lee, S.-K.; Nesheim, J. C.; Lipscomb, J. D. *J. Biol. Chem.* **1993**, *268*, 21569−21577.
(15) Lee, S.-K.; Fox, B. G.; Froland, W. A.; Lipscomb, J. D.; Munck, E. *J. Am. Chem. Soc.* **1993**, *115*, 6450−6451.
(16) Bollinger, J. M., Jr.; Edmondson, D. E.; Huynh, B. H.; Filley, J.; Norton, J. R.; Stubbe, J. *Science* **1991**, *253*, 292−298.

10.1021/ja9824270 CCC: $15.00
Published on Web 12/01/1998

environment surrounding the metal ions contributes to the reactivity toward O_2. An essential step in this process is to establish their structure(s). The present studies use rapid freeze-quench (RFQ) ENDOR spectroscopy of **X** that is ^{17}O-labeled with $H_2{}^{17}O$ and $^{17}O_2$ to further elucidate its structure.

The early studies of Atkin et al.[19] demonstrated that incubation of apo-R2 with Fe^{II}, O_2, and reductant results in the formation of the catalytically essential, stable ·Y122 and diferric cluster. These experiments provided the groundwork for a detailed examination of the assembly reaction using stopped-flow UV−vis spectroscopy and RFQ EPR and Mössbauer spectroscopies.[16,17,20] These studies first revealed the paramagnetic intermediate **X** and its kinetic competence in the oxidation of Y122.[17]

EPR, ENDOR, and EXAFS spectroscopies have shed important light on the structure of **X**. EPR spectroscopic studies of **X** in both wild-type (wt) R2 and the mutant Y122F R2 revealed a narrow, nearly isotropic signal at $g = 2.00$ which was broadened in the presence of $^{17}O_2$ and $H_2{}^{17}O$.[20] These studies, however, were unable to accurately determine the number of oxygens associated with **X** due to the low enrichment of the ^{17}O labels used.

RFQ ^{57}Fe Q-band ENDOR studies led to the formulation of **X** as a spin-coupled Fe^{III}/Fe^{IV} center, with an $S = {}^1/_2$ ground state.[18] An extensive set of CW and pulsed Q-band $^{1,2}H$ ENDOR measurements then led to the conclusion that **X** contains a single terminal aqua ligand (water molecule or 2-fold disordered hydroxyl) bound to Fe^{III} and does not contain a hydroxyl bridge.[21]

Recent RFQ-EXAFS experiments on **X** generated with both wt R2 and Y122F R2 revealed a very short Fe−Fe distance of 2.49 Å, as well as at least one short Fe−O bond of 1.8 Å.[22] ENDOR and EXAFS data, plus the strong spin coupling between the iron ions, constrain the structure of **X** to a $[(H_xO)Fe^{III}OFe^{IV}]$ core with one or possibly two additional mono-oxo bridges. Finally, the resonance Raman studies of Ling et al.[23] on Y122F R2 revealed that O_2 is the predominant source of the bridging μ-oxo-oxygen in the final diferric cluster. Similar experiments have thus far not been reported for the wt R2, but, based on the structural similarities in the two proteins, it presumably will give the same results.[24] Thus, it is likely that **X** contains at least one μ-oxo bridge derived from O_2 gas.

To determine the number of oxo bridges in the core and to establish the fate of the atoms derived from O_2 requires ^{17}O ENDOR experiments on samples of **X** prepared in both $H_2{}^{17}O$ and $^{17}O_2$. Our initial CW ENDOR examination of such samples detected ^{17}O signals, suggestive that three oxygen atoms might be associated with **X**: one oxygen derived from solvent; one derived from dioxygen, with a large hyperfine coupling; and possibly a second derived from dioxygen, with a small coupling.[25] The present ^{17}O ENDOR study employs natural abundance and uniformly ^{15}N-labeled protein, [U-^{15}N]-R2, in both CW *and* pulsed ENDOR experiments, to further elucidate the structure of **X**. These measurements, which include kinetic studies of the formation of **X** in both wt and Y122F R2 as monitored by both ENDOR and S-band EPR spectroscopies, reveal that **X** contains two oxygen atoms. Both are initially derived from O_2, with one present as a μ-oxo bridge and one as the terminal aqua ligand, and with time the latter of these atoms exchanges with solvent. These and our previous studies suggest that **X** does not contain a di-μ-oxo or μ-oxo,hydroxo bridge structure such as that recently proposed for **Q** in MMOH.[26] A structure for **X** is proposed that contains a single oxo bridge, one terminal aquo/hydroxo ligand bound to the Fe^{III}, and one or two additional mono-oxo bridges provided by the carboxylate oxygens of E115 and/or E238 ligands to the cluster.[10,11] In addition, the time course of the formation of **X** in the presence of $^{17}O_2$ provides important insights into the dynamics of cluster assembly.

Materials and Methods

Materials. $^{17}O_2$ gas (85.5%) and $H_2{}^{17}O$ (34.9%) were purchased from Isotec. $^{15}NH_4SO_4$ (98%) and $H_2{}^{17}O$ (35.9%) were purchased from Cambridge Isotope Laboratories.

Overproduction of Apo-[U-^{15}N] Y122F. [U-^{15}N]-R2-Y122F was isolated from the overproducing strain BL21(DE3)/pTB2(Y122F)Y122[17] using a glycerol-based minimal medium with $(^{15}NH_4)_2SO_4$ as the sole nitrogen source. Glycerol (40 g), 3.2 g of KH_2PO_4, and 20 g of $Na_2HPO_4{\cdot}7H_2O$ were added to 2 L of H_2O in a 6-L flask and were sterilized. Upon cooling, the following filtered sterilized solutions were added: (1) a 10-mL solution containing sodium citrate (1.0 g), $MgSO_4$ (0.60 g), and $(^{15}NH_4)_2SO_4$ (4.0 g); (2) a 3-mL solution containing the trace salts $FeCl_3{\cdot}6H_2O$ (99 mg), $ZnSO_4{\cdot}7H_2O$ (0.54 mg), $CuSO_4{\cdot}6H_2O$ (0.48 mg), $CoCl_2{\cdot}6H_2O$ (0.54 mg), $CaCl_2{\cdot}2H_2O$ (1.5 mg), and Na_2-EDTA (114 mg); and (3) a 20-mL solution containing the cofactors biotin (0.04 mg), folic acid (0.04 mg), Ca^{2+} pantothenate (0.1 mg), vitamin B12 (0.002 mg), nicotinamide (0.1 mg), and riboflavin (0.1 mg). Ampicillin (100 mg) and thiamine-HCl (10 mg) were added prior to inoculation with 50 mL of a saturated cell culture. The cells were grown at 37 °C to an OD_{600} of 0.9 and were induced by the addition of isopropyl β-D-thiogalactopyranoside to a final concentration of 0.5 mM. Cell growth was continued for an additional 4 h, reaching a final OD_{600} of 1.3. The cells were harvested by centrifugation, yielding 8.5 g of frozen cell paste for a 4-L growth.

Preparation of Apo-[U-^{15}N]-Y122F R2. [U-^{15}N]-Y122F R2 was isolated by procedures described previously,[17] yielding 180 mg of protein from the 8.5 g of cell paste. Apo-[U-^{15}N]-Y122F R2 was prepared from the native protein using the method of Atkin et al.[19] The concentration of apo-Y122F R2 was determined from A_{280} (ϵ = 120 mM^{-1} cm^{-1}).[27]

Preparation of RFQ Q-Band ENDOR Sample of [U-^{15}N]-Y122F R2 in $^{17}O_2$-Saturated Buffer. The method for preparing this doubly labeled sample is the same as that previously described.[18] The RFQ instrument consists of an Update Instruments Drive Ram assembly, a model 715 computer controller, and a quenching bath. One drive syringe of the ram unit was filled with apo-Y122F R2 (512 μM) in argon-saturated Hepes (100 mM, pH 7.7), while the other was loaded with a solution of Fe^{2+} (2.70 mM) in $^{17}O_2$-saturated 5 mN H_2SO_4. The reaction was quenched at 610 ms to maximize the amount of **X**. The quench employed isopentane at approximately its melting temperature (114−118 K), and the Q-band ENDOR tubes were packed at this temperature. The preparations described below also used the isopentane quench technique. Between experiments, samples were stored in liquid nitrogen.

(17) Bollinger, J. M., Jr.; Tong, W. H.; Ravi, N.; Huynh, B. H.; Edmondson, D. E.; Stubbe, J. *J. Am. Chem. Soc.* **1994**, *116*, 8015−8023.
(18) Sturgeon, B. E.; Burdi, D.; Chen, S.; Huynh, B. H.; Edmondson, D. E.; Stubbe, J.; Hoffman, B. M. *J. Am. Chem. Soc.* **1996**, *118*, 7551−7557.
(19) Atkin, C. L.; Thelander, L.; Reichard, P.; Lang, G. *J. Biol. Chem.* **1973**, *248*, 7464−7472.
(20) Ravi, N.; Bollinger, J. M., Jr.; Huynh, B. H.; Edmondson, D. E.; Stubbe, J. *J. Am. Chem. Soc.* **1994**, *116*, 8007−8014.
(21) Willems, J.-P.; Burdi, D.; Lee, H.-I.; Doan, P. E.; Stubbe, J.; Hoffman, B. M. *J. Am. Chem. Soc.* **1997**, 9816−9824.
(22) Riggs-Gelasco, P. J.; Shu, L.; Chen, S.; Burdi, D.; Huynh, B. H.; Que, L., Jr.; Stubbe, J. *J. Am. Chem. Soc.* **1998**, *120*, 849−860.
(23) Ling, J.; Sahlin, M.; Sjöberg, B.-M.; Loehr, T. M.; Sanders-Loehr, J. *J. Biol. Chem.* **1994**, *269*, 5595−5601.
(24) Tong, W.; Burdi, D.; Riggs-Gelasco, P.; Chen, S.; Edmondson, D. E.; Huynh, B. H.; Stubbe, J.; Han, S.; Arvai, A.; Tainer, J. *Biochemistry* **1998**, *37*, 5840−5848.
(25) Burdi, D.; Sturgeon, B. E.; Tong, W. H.; Stubbe, J.; Hoffman, B. M. *J. Am. Chem. Soc.* **1996**, *118*, 281−282.
(26) Shu, L. J.; Nesheim, J. C.; Kauffmann, K.; Munck, E.; Libscomb, J. D.; Que, L. *Science* **1997**, *275*, 515−518.
(27) Thelander, L. *J. Biol. Chem.* **1973**, *248*, 4591−4601.

Preparation of RFQ Q-Band ENDOR Sample of [U-^{15}N]-Y122F R2 in $H_2{}^{17}O$-Enriched Buffer. One drive syringe of the ram unit was filled with apo-Y122F R2 (485 μM) in $^{16}O_2$-saturated Hepes buffer (100 mM, pH 7.7) that was 26% enriched with $H_2{}^{17}O$. The other syringe was filled with an Fe^{2+} solution in $^{16}O_2$-saturated 5 mN H_2SO_4 enriched with 35% $H_2{}^{17}O$. The reaction was quenched at 610 ms.

Preparation of $^{17}O_2$-Saturated Solutions. An aqueous solution (4 mL) containing either buffer or Fe^{2+} in 5 mN H_2SO_4 was placed in a 10-mL round-bottomed flask equipped with a vacuum inlet and septa cap. The solutions were subjected to four cycles of freeze−pump−thaw and then connected to a capillary manometer/manifold assembly. $^{17}O_2$ gas was admitted to the evacuated flask to a pressure of 1.1 atm, and the flask was sealed and allowed to stand overnight at 5 °C.

Preparation of RFQ Q-Band ENDOR and S-Band EPR Samples of Y122F R2 in $^{17}O_2$-Saturated Buffer. EPR samples were prepared using the RFQ techniques described previously.[28−30] One drive syringe of the ram assembly was loaded in an anaerobic glovebox with diferrous-Y122F R2 (600 μM apo-Y122F R2, 3.0 mM $FeSO_4$) in Hepes buffer (100 mM, pH 7.7). The other syringe was loaded with $^{17}O_2$-saturated Hepes buffer (100 mM, pH 7.7). The reaction times were varied from 28 to 4030 ms by choosing the appropriate length aging loop.

Preparation of RFQ Q-Band ENDOR Samples of Y122F R2 in $H_2{}^{17}O$-Enriched Buffer. Solutions of 8.75 mM $FeSO_4$ in 10.7 mN H_2SO_4 enriched with 29.1% $H_2{}^{17}O$, 1.62 mM apo-Y122F R2, and 34.4% $H_2{}^{17}O$-enriched 100 mM Hepes buffer (pH 7.6) were degassed, placed in a glovebox, and combined to give a solution of 525 μM Y122F R2 and 2.63 mM Fe^{2+} with a final $H_2{}^{17}O$ enrichment of 28.1%. The anaerobic solution was then loaded into one of the drive syringes. $^{16}O_2$-Saturated Hepes buffer (100 mM, pH 7.6, 4 °C) enriched with 34.4% $H_2{}^{17}O$ was loaded into the second drive syringe. The solutions were mixed and quenched by rapid freezing for either 42 or 4 s.

ENDOR Spectroscopy. The CW ENDOR spectrometer, which employs 100-kHz field modulation, has been briefly described;[31] the CW ENDOR spectra are induced by a "packet-shifting" mechanism.[32] A description of the 35-GHz pulse ENDOR spectrometer employed in this study has been published recently.[33]

Given that the system under study is a transient intermediate, the spectrometer cavity was immersed in liquid nitrogen during sample insertion, so as to prevent warming of the sample. There was no detectable difference between multiple samples of the same type, and each sample was run multiple times with no change in characteristics. These observations show that the results reported are not compromised by variability in the actual quench process and confirm that there are no artifacts due to warming and consequent annealling. Indeed, any sample freeze-quenched in isopentane, stored in liquid nitrogen, and subsequently warmed to roughly the melting temperatue of isopentane (a temperature too low for protein structural reorganizations) is likely to explode.

For a paramagnetic center in a frozen solution, the first-order ENDOR signal from a particular nucleus is a well-defined superposition of patterns comprised of two branches whose frequencies are given by[34,35]

$$\begin{aligned} \nu_\pm &= |\nu_L \pm {}^1/_2 A| \qquad \text{for } I = {}^1/_2 \\ \nu_\pm &= |\nu_L \pm {}^1/_2 A + {}^1/_2 P(2m_i - 1)| \qquad \text{for } I > {}^1/_2 \end{aligned} \tag{1}$$

where A and P are the hyperfine and quadrupole couplings for a particular orientation, ν_L is the nuclear Larmor frequency, and $m_i = I, I - 1, ..., -I$.

The majority of the pulsed ENDOR spectra reported here were collected with the Davies ENDOR pulse sequence ($\pi - T - \pi/2 - \tau - \pi$; rf applied during T).[36] It is hyperfine-selective in that the ENDOR response, R, is jointly dependent on the hyperfine coupling, A, and the length of the preparation microwave pulse, t_p, in the preparation phase, through the selectivity factor, $\eta = At_p$:

$$R = R_0\left(\frac{1.4\eta}{0.7^2 + \eta^2}\right) \tag{2}$$

where R_0 is the maximum ENDOR response. The equation shows that an optimal ENDOR response is obtained if $\eta = At_p = 0.7$; when $\eta < 0.7$, the response is suppressed. For a given sample, the value of t_p cannot be lengthened beyond some *intrinsic* maximum, $t_p{}^{max}$, because dephasing during the pulse diminishes or abolishes the spin−echo observed in the detection phase of the experiment. As a result, the smallest hyperfine coupling, A^{min}, that can be observed with sufficient signal-to-noise ratios (S/N) using a Davies ENDOR sequence is roughly $A^{min} \approx 1/t_p{}^{max}$; signals from nuclei having a hyperfine coupling less than this value will be severely suppressed. In the case of **X**, the maximum useful value of t_p typically was of the order of 0.2 μs, which means that an optimized Davies ENDOR response could be achieved for nuclei having hyperfine coupling constants larger than ~3.5 MHz.

To assign some ^{17}O signals, a few of the oxygen ENDOR spectra were collected using the ReMims four-pulse stimulated-echo ENDOR pulse sequence ($^1/_2\pi - \tau - {}^1/_2\pi - T - {}^1/_2\pi - \tau_2 - \pi - [\tau + \tau_2]$−echo; rf applied during T).[37] This protocol also is hyperfine-selective in that its ENDOR response R depends jointly on the nuclear hyperfine coupling A and the interval τ according to

$$R \propto [1 - \cos(2\pi A\tau)] \tag{3}$$

This equation shows that the ENDOR response will fall to zero for $A\tau = 0, 1, 2, ...$, and will reach a maximum for $A\tau = 0.5, 1.5, ...$ In the presented study, the minimum τ value used was 164 ns, resulting in a maximum hyperfine value, A^{max}, which can be observed without distortions, of 3 MHz.

As reviewed in detail,[32,38,39] the full hyperfine tensor of an interacting nucleus, including both the principal values and the orientation relative to the **g** tensor, was determined by collecting a 2-D ENDOR dataset comprised of spectra collected at multiple fields across the EPR envelope and comparing them to simulated 2-D patterns. In many cases, including the present ^{17}O ENDOR measurements, CW ENDOR spectra exhibit better S/N ratios than do pulsed ENDOR ones, and thus it was desirable to use the CW protocol in generating the 2-D patterns. However, in interpreting these patterns, it is essential to have spectra with undistorted line shapes. At low temperature, where relaxation rates are slow, the CW line shapes and intensities depend on the spectrometer settings, such as microwave power, field modulation amplitude, rf power, and rf scan rate and direction, largely because of slow relaxation of the nuclear spins. To take advantage of the sensitivity of the CW method, ^{17}O ENDOR spectra were first recorded by the Davies pulsed ENDOR protocol, which does give reliable shapes. The instrument settings in the CW spectrometer were then set so that the CW signals reliably matched those obtained using the Davies technique. The settings are given in the appropriate figure legends. The exception to this procedure is that, for various instrumental reasons (e.g., a better impedance matching of the rf circuit at lower frequencies), the pulsed ENDOR methods appear to be more sensitive to signals at low frequencies ($\nu \lesssim 8$ MHz). In those 2-D patterns where the characteristics of the low-frequency ENDOR response are of particular importance, the Davies pulsed ENDOR technique was used.

(28) Bollinger, J. M. J.; Tong, W. H.; Ravi, N.; Huynh, B. H.; Edmondson, D. E.; Stubbe, J. *Methods Enzymol.* **1995**, *258*, 278−303.
(29) Bray, R. C. *Biochem. J.* **1961**, *81*, 189.
(30) Ballou, D. P.; Palmer, G. *Anal. Chem.* **1974**, *46*, 1248.
(31) Werst, M. M.; Davoust, C. E.; Hoffman, B. M. *J. Am. Chem. Soc* **1991**, *113*, 1533−1538.
(32) DeRose, V. J.; Hoffman, B. M. *Methods Enzymol.* **1995**, *246*, 554−589.
(33) Davoust, C. E.; Doan, P. E.; Hoffman, B. M. *J. Magn. Reson., A* **1996**, *119*, 38−44.
(34) Abragam, A.; Bleaney, B. *Electron Paramagnetic Resonance of Transition Ions*, 2nd ed.; Clarendon Press: Oxford, 1970.
(35) Atherton, N. M. *Electron Spin Resonance. Theory and applications*; Halsted Press: New York, London, Sydney, Toronto, 1973.
(36) Davies, E. R. *Phys. Lett* **1974**, *47A*, 1−2.
(37) Doan, P. E.; Hoffman, B. M. *Chem. Phys. Lett.* **1997**, *269*, 208−214.
(38) Hoffman, B. M. *Acc. Chem. Res.* **1991**, *24*, 164−170.
(39) Hoffman, B. M.; DeRose, V. J.; Doan, P. E.; Gurbiel, R. J.; Houseman, A. L. P.; Telser, J. *Biol. Magn. Reson.* **1993**, *13*, 151−218.

The simulations of the ENDOR spectra described in this paper followed the strategies we have described earlier, and that will be described below. However, they were performed using a program (DDPOWHE) which utilizes exact diagonalization routines to calculate the orientation-dependent nuclear spin energies, rather than perturbation theory formulas. The intensities of the ν_- transitions are higher in the simulations than they are in the experimental data, because of transition probability terms not included in the simulations. As a result, the ν_- intensities of spectra presented here have, in some cases (see figure legends), been arbitrarily scaled to best match experiment. EPR spectra were simulated with the program QPOW.[40]

S-Band EPR Spectroscopy. EPR experiments at S-band (3.4 GHz) were performed with loop-gap resonators and low-frequency microwave bridges designed and built at the National Biomedical ESR Center at the Medical College of Wisconsin.

Results

Mutant Y122F R2 versus Wild-Type R2. The EPR spectra of **X** and the tyrosyl radical overlap, and thus RFQ ENDOR experiments can be successfully performed only when **X** alone is present in the samples. The kinetics of the assembly of cofactor with the wt R2 have thus been limited to early time points (<100 ms) when **X** has not yet given rise to ·Y. To examine a time course of cluster assembly by RFQ ENDOR, we have therefore focused most of our studies on Y122F R2, in which the tyrosine is replaced by the nonoxidizable phenylalanine.[41] To establish the validity of this approach, we have compared ^{57}Fe, ^{14}N, and ^{1,2}H ENDOR measurements of **X** in the mutant (prior studies[18,21] and data not shown) and wild-type (data not shown) protein: they disclose *no* structural differences between **X**(wt) and **X**(Y122F). Comparisons of ^{17}O measurements are presented below.

Characterization of ^{17}O ENDOR Signals by Multiple ENDOR Techniques. As reported by Burdi et al.,[25] the Q-band ENDOR spectra of **X** show ^{14}N signals from the coordinated nitrogen atoms of the histidine ligands in the frequency range $4 \lesssim \nu \lesssim 15$ MHz (Figure 1). They also show proton resonances at frequencies above ~40 MHz (not shown). For natural-abundance samples, no signals are seen at intermediate frequencies, but as reported earlier, the CW ENDOR spectra of the $H_2{}^{17}O$- and $^{17}O_2$-enriched samples both show ^{17}O signals in the frequency range $13 < \nu < 25$ MHz, associated with hyperfine couplings in the range from 20 to 35 MHz (Figure 1). The absence of any ^{17}O signals to higher frequencies shows that, for both types of labels, the ^{17}O resonances in the region of ~13−25 MHz must be associated with ν_+ transitions of ^{17}O. The shapes of the CW signals are distinctly different for the two types of sample, as shown in Figure 1, but they do appear in the same frequency range. It could not be unambiguously ascertained whether the observed differences are the results of different hyperfine/quadrupole parameters for two distinct types of site or merely distortions that arise from slow electron and nuclear relaxation processes. Properly performed pulsed ENDOR spectra do not suffer such distortions, and we have thus used Davies pulsed ENDOR measurements at Q-band to confirm the shapes of the ^{17}O signals from **X**. In fact, the ^{17}O CW signal from the $^{17}O_2$ sample faithfully reproduces the shape of the pulsed ENDOR signal, but with better S/N. It is centered at ~20 MHz; it has a well-defined breadth from quadrupolar interactions (eq 1) of about 7 MHz, with the low-frequency edge appreciably more intense. The pulsed ENDOR signal from the $H_2{}^{17}O$-enriched sample corroborates the essential features of the

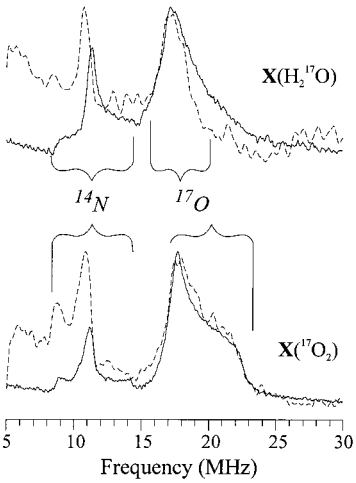

Figure 1. 35-GHz CW (—) and Davies pulsed (- - -) ENDOR spectra taken at $g = 1.994$ for mutant **X**($H_2{}^{17}O$) (upper) and **X**($^{17}O_2$) (lower); both samples are quenched at 4030 ms. Upper: sample prepared with $H_2{}^{17}O$ (30% isotope enrichment); lower, sample prepared with $^{17}O_2$ (85% isotope enrichment). Experimental conditions: CW, microwave frequency 35.1603 (upper), 35.1742 (lower) GHz, modulation amplitude 8 G; rf scan speed 1 MHz/s; the rf is swept from low to high frequencies; pulsed spectrum, microwave frequency 34.852 (upper), 34.887 (lower) GHz, microwave π pulse width 200 ns, rf pulse width 60 μs. Temperature, 2 K.

CW spectrum. It consists of a single narrow (~2 MHz) peak at ~18 MHz, without appreciable quadrupolar breadth. The only distortion in the CW spectrum is a trailing to high frequency that results from slow nuclear relaxation and does not compromise analysis.[42] In the absence of the pulsed ENDOR confirmation, however, we could not be sure that the trailing edge of the narrow signal in the $H_2{}^{17}O$ was not, in fact, a distorted version of the broad peak seen in the $^{17}O_2$ sample. Figure 1 shows that this clearly is not the case, and the two types of label give rise to sites with distinctly different ENDOR patterns.

In our previous CW study[25] of the sample prepared with $^{17}O_2$, an additional ^{17}O signal was detected at ~9 MHz. The presence of this feature, combined with the absence of a similar one in the sample prepared with $H_2{}^{17}O$, led to the proposal that it represented the ν_+ branch of a second oxygen atom from O_2, denoted O_b, rather than the ν_- branch from a single species whose ν_+ branch is seen at higher frequencies. From eq 1, the hyperfine value for such an O_b signal then would be less than ~3.5 MHz. The hyperfine selectivity of the Davies (eq 2) and ReMims (eq 3) pulsed ENDOR measurements gives us a means of deciding unambiguously whether the ^{17}O ENDOR intensity at 9 MHz is from an ^{17}O nucleus with $A \approx 3.5$ MHz. A ReMims sequence with $\tau \approx 140$ ns would maximize such a signal, while a Davies measurement with $t_p \approx 200$ ns would suppress it. The reverse is true if the intensity at 9 MHz is from the ν_- partner of an ^{17}O with the ν_+ branch at 20 MHz, and thus $A \approx 22$ MHz.

Figure 2 shows Davies (top spectra) and ReMims (bottom spectra) pulsed ENDOR spectra taken at a field position corresponding to g_2 for samples prepared both with $^{17}O_2$ (left) and $H_2{}^{17}O$ (right). The measurements employ samples doubly labeled with ^{15}N and ^{17}O, because ^{14}N signals from histidine that fall in the range 7−12 MHz otherwise would obscure the ^{17}O signals. The isotopic replacement increases the frequencies from the nitrogen ligands by a factor of $g^{15}_N/g^{14}_N = 1.4$, which

(40) Nilges, M. J. In *Electron Paramagnetic Resonance Studies of Low Symmetry Nickel(I) and Molybdenum(V) Complexes*; Nilges, M. J., Ed.; University of Illinois: Urbana−Champaign, IL, 1979.

(41) Larsson, Å.; Sjöberg, B.-M. *EMBO J.* **1986**, *5*, 2037−2040.

(42) Slight shifts seen in the CW ^{14}N peak positions are sweep-related and are readily accommodated by averaging the frequencies measured from spectra taken with positive and negative sweeps.

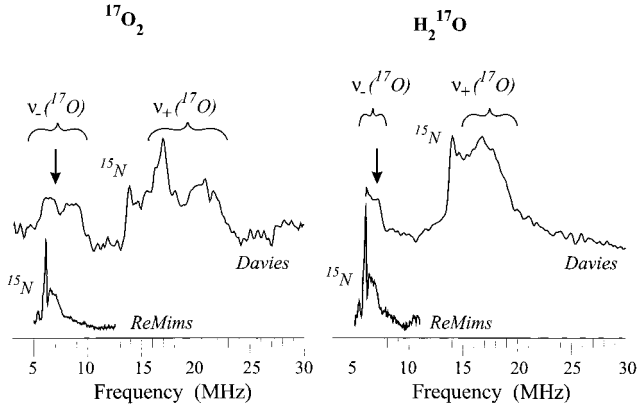

Figure 2. Pulsed ENDOR spectra taken at g_2 for two samples of mutant **X** quenched at 610 ms. Left: The sample is doubly labeled with $^{17}O_2$ and ^{15}N. Right: The sample is doubly labeled with $H_2{}^{17}O$ and ^{15}N. The top spectra have been recorded using a Davies sequence, and the bottom spectra have been taken employing a ReMims pulse sequence. The ^{17}O Larmor frequency has been indicated by an arrow. Conditions: ReMims, microwave frequency 34.902 GHz, τ = 164 ns, microwave pulse width 28 ns, rf pulse width 60 μs; Davies, microwave frequency 34.901 GHz, microwave π pulse width 200 ns, rf pulse width 60 μs. Temperature, 2 K.

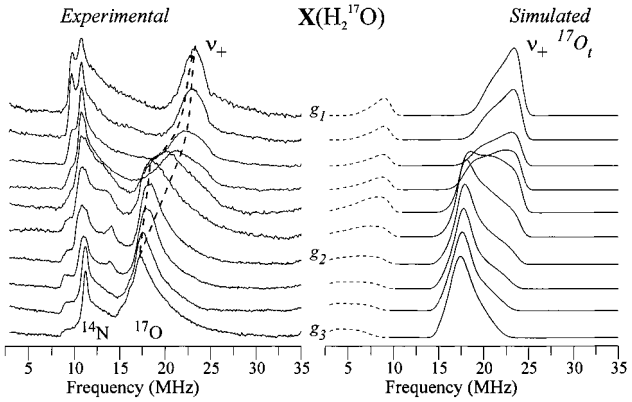

Figure 3. Field dependence of the CW ENDOR pattern of mutant **X** labeled with $H_2{}^{17}O$ and quenched at 4030 ms. Left, experimental pattern; right, simulated ^{17}O pattern. Experimental conditions: microwave frequency 35.315 GHz, modulation amplitude 8 G, modulation frequency 100 kHz, rf scan speed 1 MHz/s. The rf frequency has been swept starting at the low-frequency edge and going toward the high-frequency edge. Temperature, 2 K. Simulations: The spectral parameters used for the simulations are listed in the left column of Table 1. The ν_- transitions are indicated by the dashed lines; the intensities of these transitions have been artificially reduced in the simulated spectra in order to match the weak intensity of the corresponding signals in the experimental spectra (see Materials and Methods).

shifts the ligand nitrogen signals to ~13 MHz and higher and leaves the frequency from ~7 to ~14 MHz open for unambiguous characterization of any low-frequency ^{17}O signals.

The ReMims spectra of both the $^{15}N/^{17}O$-enriched enzyme samples, taken to maximize signals with $A \lesssim 3$ MHz, display signals from (two) weakly coupled nitrogen atoms, centered around the ^{15}N Larmor frequency ($\nu^{15}_N = 5.4$ MHz). There are no ^{17}O signals in this range for either sample. The Davies ENDOR spectrum of the same sample shows a strong additional ^{17}O feature between 5 and 10 MHz, which corresponds to that seen previously in the CW ENDOR. The Davies spectrum of the $H_2{}^{17}O$ sample shows ^{17}O intensity below ~ 7 MHz that could not be seen previously.

By the above arguments, neither the $^{17}O_2$ nor the $H_2{}^{17}O$ sample contains a weakly coupled ^{17}O. The signals at ~9 MHz and below in each case must be associated with the ν_- branch for a strongly coupled oxygen atom whose ν_+ transition is seen at higher frequencies. That oxygen in the $^{17}O_2$ sample is denoted $^{17}O_{br}$; that in the $H_2{}^{17}O$ sample is denoted $^{17}O_t$.

Characterization of X Generated in $H_2{}^{17}O$. Figure 3 shows a 2-D CW ENDOR dataset comprised of spectra taken across the EPR envelope of **X** prepared in buffer enriched in $H_2{}^{17}O$ to 30% and quenched at 4030 ms. The conditions under which the CW spectra were recorded were chosen so that the shapes of the ^{17}O signals match well with those of Davies pulsed ENDOR spectra. The peak of the ν_+ ^{17}O ENDOR signal seen at g_3 occurs at 18 MHz. As g is increased, the frequency of the intensity maximum of the ν_+ feature remains essentially invariant, while the pattern gradually extends toward higher frequency, reaching ~24 MHz by g_2. As g is further increased toward g_1, the intensity at ~24 MHz rapidly builds, while the low-frequency edge of the pattern decreases in intensity and shifts to higher frequency. To a first approximation, this is the typical 2-D pattern expected for an approximately axial hyperfine tensor with the unique axis lying along g_1: $A_\parallel = A_1 \approx 35$ MHz and $A_\perp = A_2 = A_3 \approx 20$ MHz, where all components have the same sign. This sign has not been determined but is arbitrarily taken as positive. Detailed simulations that include the ^{17}O quadrupole interaction change this analysis only modestly, the major difference being along g_3. Initially, the **A** and **P** tensors were kept collinear in the simulations. The initial estimates of the principal hyperfine component, which were close to those just mentioned, were determined from the frequencies of the maximum intensities of the ^{17}O ENDOR signals at g_1, g_2, and g_3. The maximum breadths of the ^{17}O ENDOR features were attributed to unresolved quadrupole splittings and used to obtain initial estimates for the principal values of the quadrupole tensor, the P_i. A rotation of the quadrupole tensor about the g_1 axis, causing noncollinear **A** and **P** tensors, led to a significant improvement in the fit between the simulated and experimental ENDOR patterns. Almost the last step in the simulation process was to introduce a minor rotation of the hyperfine tensor which modestly improved the fit.

The resulting hyperfine and quadrupole tensors, listed in Table 1, along with their estimated uncertainties, generate simulations in excellent agreement with experiment (right side, Figure 3). The isotropic portion of the hyperfine tensor is $A_{iso} = 23.8$ MHz. The direction of the largest tensor component, A_1, deviates slightly from g_1, lying in the g_1,g_3 plane. The result $A_1 > A_{iso}$ requires that the isotropic and largest anisotropic contributions have the same sign. Although the spectra presented in Figure 3 are comparable to those presented earlier,[25] the reported A_3 component of the hyperfine tensor differs because the quadrupole interactions are not small, and we here have employed exact solutions of the nuclear energies, rather than perturbation solutions, as were used previously.

We assign the O_t derived from solvent as the single terminal H_xO bound to Fe^{III} whose presence was deduced from our $^{1,2}H$ ENDOR measurements.[21] Indeed, the $^{17}O_t$ ENDOR data confirm that **X** does not have two aquo/hydroxy molecules terminally attached to Fe^{III}, and that **X** does not have an aqua ligand bound to Fe^{IV}. Two terminal ^{17}O atoms attached to Fe^{III} would have different orientations of their hyperfine and quadrupole tensors, which is not observed experimentally (Figure 3). It is not possible for two O_t ligands, one on each of the two Fe ions, to have identical hyperfine tensors. Their inequivalence is ensured not merely by bonding effects due to chemical inequivalence, but by the spin coupling between Fe ions: the intrinsic hyperfine

Table 1. Principal Values and Orientations of the ^{17}O Hyperfine (A_i) and Quadrupole (P_i) Tensors Determined for **X** in Y122F R2 Quenched at 4 s[a]

	$^{17}O_t$	$^{17}O_{br}$
A_1 (MHz)	34.0	0[b]
A_2 (MHz)	20.5	23.5
A_3 (MHz)	17	22.5
α (deg)	0	40
β (deg)	20	0
γ (deg)	0	0
P_1 (MHz)	−0.05	−0.60
P_2 (MHz)	−0.25	−0.80
P_3 (MHz)	0.30	1.4
α (deg)	90[c]	25
β (deg)	45	45
γ (deg)	90	0

[a] The EPR line width (fwmh) used in ENDOR simulations was 35 MHz; the ENDOR line width (fwmh) was taken to be 0.5 MHz. Euler angles are relative to the **g** tensor frame. The accuracy of the principal *A* values was better than ±0.5 MHz, except as noted, and that of the *P* values was better than ±0.05 MHz. The "non-zero" Euler angles could be determined to better than ±5°. A "zero" Euler angle is uncertain to ±10°. [b] The accuracy of A_1 is ∼±1 MHz. [c] Note that the α,γ values make this set of angles correspond to a simple rotation of β about the g_1 axis.

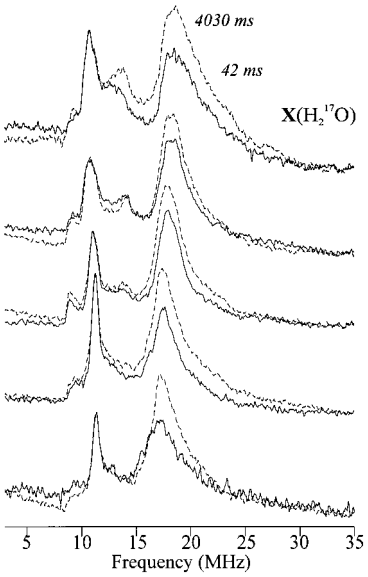

Figure 4. Pairs of 35-GHz CW ENDOR spectra taken at fields across the EPR envelope of mutant **X**($H_2{}^{17}O$). Dashed spectra, quench time 4030 ms; solid spectra, quench time 42 ms. The spectra have been recorded at magnetic field positions between g_2 (uppermost spectrum) and g_3 (lowermost); for comparison to the full field dependence, see Figure 3. Experimental conditions are as in Figure 3.

couplings of a ligand bound to Fe^{III} is multiplied by the coupling $^7/_3$, while one bound to Fe^{IV} is multiplied by $-^4/_3$.[18]

To obtain information about the kinetics of the appearance of the $^{17}O_t$ ENDOR signal, we measured the Davies (data not shown) and CW (Figure 4) ^{17}O ENDOR signals for a $H_2{}^{17}O$-labeled sample quenched at 42 ms. Both techniques show that the frequency and shape of the $^{17}O_t$ signal from this sample are the same as those for the signal quenched at 4030 ms, although the 42-ms signal is lower in intensity. The intensities of the $^{17}O_t$ signals at these two times can be compared accurately by normalizing them to the ^{14}N ENDOR signals from the histidyl ligands. The observed differences in intensities indicate that oxygen from solvent is exchanging into **X**. Further kinetic analysis of data taken from samples quenched at multiple intermediate times (data not shown) indicates that roughly half the exchange occurs within ∼40 ms after mixing, with the remainder being complete within several seconds. The basis for the biphasic exchange kinetics for **X**, and whether it reflects exchange from a precursor to **X** or is associated with more than one form of **X**, will be discussed subsequently.

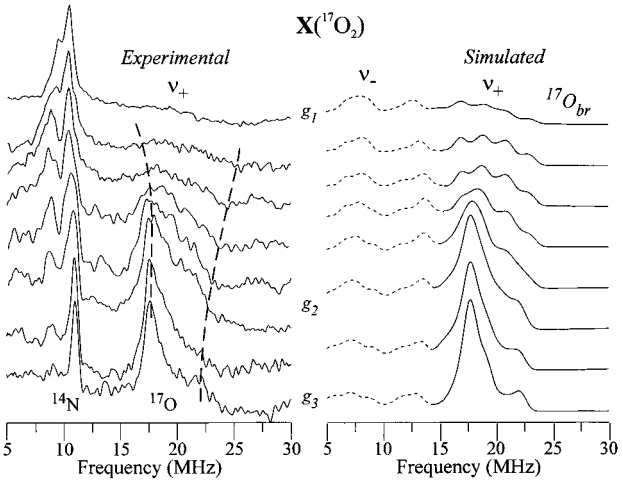

Figure 5. Left: Davies pulsed ENDOR spectra taken across the EPR envelope for mutant **X**($^{17}O_2$) quenched at 4030 ms. Experimental conditions: Davies pulse sequence, microwave frequency 34.887 GHz, τ = 512 ns, microwave π pulse width 200 ns, rf pulse width 60 μs, temperature 2 K. Right: Corresponding simulation for $^{17}O_{br}$, using the parameters of Table 1. The ν_- transitions are indicated by dashed lines because the intensities of these transitions have been artificially reduced in the simulated spectra in order to match the weak intensity of the corresponding signals in the experimental spectra.

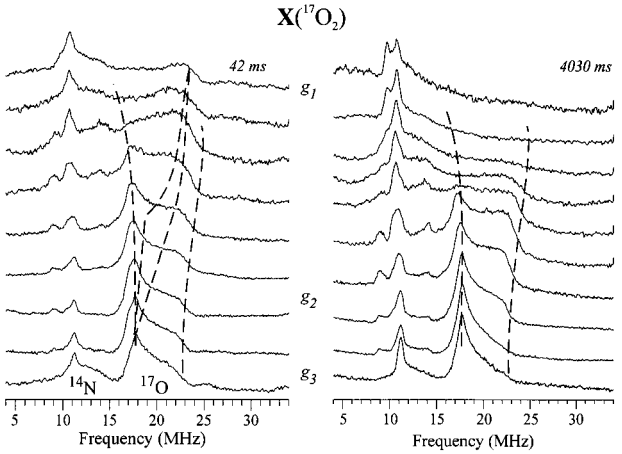

Figure 6. CW ENDOR spectra taken across the EPR envelope for two different samples of mutant **X**, both labeled with $^{17}O_2$. Quench times: 42 (left) and 4030 ms (right). Conditions: microwave frequency 35.241 GHz (42-ms quenched sample), 35.174 GHz (4030-ms sample), modulation amplitude 8 G, modulation frequency 100 kHz, rf scan speed 1 MHz/s. The rf frequency has been swept starting at the low-frequency edge. Temperature, 2 K.

Characterization of X Generated in $^{17}O_2$. A sample of **X** prepared with $^{17}O_2$ gas (85%) and Y122F R2, and quenched at 4030 ms, was analyzed by both the Davies pulsed ENDOR and CW ENDOR protocols. Full 2-D ENDOR datasets for $^{17}O_{br}$ were taken across the EPR envelope: Davies, Figure 5 (left), and CW, Figure 6 (right). The CW spectra have better S/N, and the conditions under which they were taken were selected to best reproduce the shapes in the Davies spectra (compare the two datasets, particularly between g_3 and g_2). At some fields, however (particularly for $g > g_2$), the spectra have features at low frequencies ($\nu \lesssim 8$ MHz) that are better seen using the Davies method. The pulsed ENDOR spectra were therefore chosen for analysis and simulation.

As shown in Figure 5, as the g value is raised from g_3 to g_2, the quadrupole-broadened $^{17}O_{br}$ signal between ~17 and 23 MHz loses definition and some intensity. One can detect an extension of the $^{17}O_{br}$ intensity toward lower frequency (below 15 MHz) at g values near and above g_2 through a "rise" in what appears to be baseline, but is not. Finally, as the g value is raised toward g_1, the extension of the ^{17}O signal to low frequency (and broadening) causes it to lose amplitude, until it is barely detectable by g_1. The roughly constant frequency (~17 MHz) of the strongest feature at fields between g_3 and g_2, coupled with the shift of intensity to lower frequency as g is increased through and past g_2, suggests that $^{17}O_{br}$ is roughly characterized by an axial hyperfine tensor with the unique axis along g_1, but in this case with $A_{||} = A_1 \ll A_\perp \approx A_2 \approx A_3 \approx 23$ MHz, where again we have arbitrarily set the signs as positive. The dramatic decrease in the ^{17}O ENDOR intensity as the magnetic field is changed from g_2 to g_1 could only be reproduced in the simulated ENDOR pattern with a large rotation of the hyperfine tensor about the g_3 axis (large Euler angle, α). The breadth of the ^{17}O feature in a given spectrum is governed by unresolved quadrupole splittings, but the figure further shows that the feature is unsymmetric between ~g_3 and g_2, with a maximum at the low-frequency side. This kind of asymmetry could only be reproduced in the simulations if the P_1 and P_3 components are thoroughly mixed: β(quadrupole) = 45. Therefore, the initial values for the simulations were $A_1 = 0$, $A_2 = 23$, and $A_3 = 23$ MHz; α (A tensor) = 40 and β (P tensor) = 45.

The right side of Figure 5 shows the best simulated 2-D ENDOR pattern that has been achieved; the parameters are listed in Table 1. The agreement between the simulations and the experiments again is excellent, although the smearing of the spectrum near g_1 makes the resulting A_1 and P_1 parameters less well defined. The anisotropic contribution to the hyperfine tensor is, indeed, almost axial, with the unique component lying roughly midway between g_1 and g_2. According to Table 1, the isotropic part of the hyperfine tensor is ~15 MHz, which is about two-thirds that for $^{17}O_t$ of water. Note that the observation that $A_{||} \approx 0 < A_\perp$ for $^{17}O_{br}$ implies that the isotropic and anisotropic contributions have *opposite* signs, unlike the case of $^{17}O_t$.[43] Finally, we note that the quadrupole couplings for $^{17}O_{br}$ are much different than those for $^{17}O_t$. Future work will examine these differences.

We assign O_{br} to μ-oxo bridge(s) derived from O_2 (see below).

The kinetic studies of formation of **X** in $H_2{}^{17}O$ indicated that exchange of oxygens into **X** occurred as a function of time and suggested that similar exchange should be detectable starting with $^{17}O_2$. Figure 6 shows that there are dramatic differences between the 2-D CW ENDOR pattern obtained from a sample of **X** labeled with $^{17}O_2$ and quenched at 42 ms (left) and one quenched at 4030 ms (right). These differences are seen most clearly in the spectra taken at g_1. The 42-ms sample shows a peak at ~23 MHz, whereas the sample quenched at 4030 ms does not. This additional early-time intensity, in fact, is seen throughout the 2-D pattern and must arise from the ν_+ branch of a signal associated with the second atom of O_2. This atom also has a large hyperfine coupling but clearly is exchangeable with solvent so as to be lost almost completely within 4 s. In fact, comparison of this 2-D pattern with those shown in Figures 3 and 5 indicates that the ^{17}O signals obtained from the sample quenched at 42 ms seem to be the superposition of an $^{17}O_{br}$ pattern seen at long time and the $^{17}O_t$ pattern seen in the sample prepared with $H_2{}^{17}O$. These results suggest that, when **X** is formed, it contains sites that originate from both atoms of O_2: One gives the signal denoted $^{17}O_{br}$ and does not exchange with solvent on the time scale of these experiments. The other gives a signal that is identical with that of $^{17}O_t$ from solvent and exchanges with solvent.

Correlation between ENDOR and S-Band EPR Measurements for X($^{17}O_2$) Y122F R2, and Comparison with X for wt R2. To corroborate the conclusions about the number and origin of the exogenous oxygen atoms of **X** and the exchange between solvent oxygen and oxygenic sites, we performed measurements of ^{17}O EPR linebroadening. Such measurements are incapable of *simultaneously* determining the number (N) of bound ^{17}O atoms, their occupancy (o_i), and their individual hyperfine coupling constants (A_i) because the broadening in essence depends on the occupancy-weighted sum of the anisotropic hyperfine interactions ($\sum_{i=1}^{N} o_i A_i$), convoluted over the EPR envelope. However, the ENDOR determination of the hyperfine tensors of all bound ^{17}O species makes it possible to calculate unambiguously the influence of ^{17}O enrichment on an EPR signal as a function of the number of sites and their occupancies. The interplay between the anisotropic hyperfine interaction and the g anisotropy interferes with this experiment when it is carried out at 35 GHz and, to a lesser extent, even at X-band. Thus, S-band EPR experiments were carried out because this low microwave frequency (~3.4 GHz) suppresses the effects of g anisotropy and gives the narrowest possible signals in a natural-abundance sample. It therefore maximizes the effect of broadening by ^{17}O. Nonetheless, even at S-band, the linebroadening measurements could not be analyzed reliably for **X** formed in $H_2{}^{17}O$ solvent, because of the low enrichment available (~30%). Hence we report only the measurements with the highly enriched (85%) $^{17}O_2$.

First consider the S-band spectrum of mutant **X** prepared with (85%) $^{17}O_2$ and quenched at 4030 ms (Figure 7). Simulations have been performed assuming that the intrinsic EPR line width of **X** is unaffected by the isotopic enrichment and assuming either a *single* $^{17}O_{br}$ atom (85% occupancy) with the hyperfine tensor determined by ENDOR spectroscopy (Table 1) or *two* such *identical* $^{17}O_{br}$ sites. The simulation that includes a *single* $^{17}O_{br}$ atom (Figure 7, bottom) reproduces the very obvious "shoulder" at the high-field side of this EPR spectrum, as well as "flattening" of the low-field peak of the derivative. The narrow component, most clearly seen in the negative-going, high-field half of the spectrum, is from **X** without ^{17}O label. The simulation with *two* such *identical* $^{17}O_{br}$ sites smears out both resolved features of the experiment (Figure 7, bottom). Thus, the S-band EPR and the ENDOR results for mutant **X** quenched at 4030 ms are consistent in indicating the presence of *one* O_{br} site whose oxygen atom is derived from gas.

Comparison of the S-band EPR spectrum of the mutant **X** labeled with $^{17}O_2$(85%) and quenched at 4030 ms with that quenched at 42 ms (Figure 7, top) clearly shows additional ^{17}O linebroadening at the early time point. The broadening is appreciably greater than that predicted by the simulation for two equivalent $^{17}O_{br}$ atoms just discussed. This result is consistent with expectations from the exchange phenomena seen in the ENDOR measurements. These studies indicate that, at 42 ms, the EPR spectrum should be comprised of contributions from four different isotopologs of **X**: one that has two labeled ^{17}O atoms per molecule (O_{br} and O_t), one in which only the O_{br} atom is labeled, one which only has a labeled $^{17}O_t$ atom, and one which does not have any labeled ^{17}O atom. These contributions would be expected to cause the pronounced shoulders seen

(43) We show below that O_{br} is an oxo bridge. As a result, its hyperfine tensor must be the sum of contributions with opposite signs from the spin delocalized from the two Fe ions.

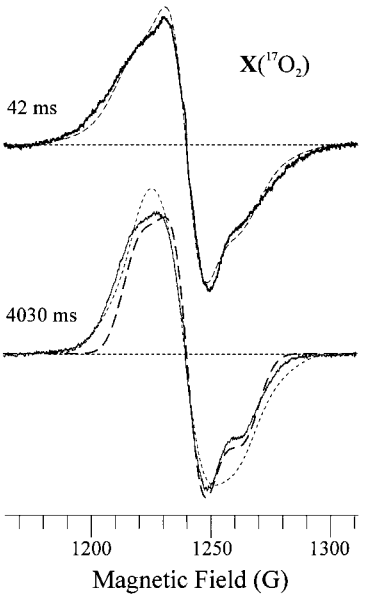

Figure 7. S-band EPR spectra for mutant **X**($^{17}O_2$) quenched at 42 ms (upper) and 4030 ms (lower). Solid lines, experimental spectra; dashed lines, simulations. The displayed spectra have been shifted slightly, as necessary, so as to have the same zero-crossing, which corresponds to that for a microwave frequency of 3.470 GHz. Simulation parameters for 4030 ms: heavy-dashed line, one $^{17}O_{br}$ (85% enrichment) having parameters listed in Table 1; short-dashed line, two $^{17}O_{br}$ (85% enrichment each), each with the $^{17}O_{br}$ parameters. For 42 ms: 40% occupancy of $^{17}O_t$, 85% of $^{17}O_{br}$ oxygens; three different conformers in a ratio of 0.2:1:0.2, where the A_3 values of $^{17}O_{br}$ in the two minority conformers are approximately 30% higher/lower than those listed in Table 1. For all: EPR line width for "terminal" oxygen, [20, 20, 40] MHz; EPR line width for bridging oxygen, [20, 20, 20] MHz. Experimental conditions: scan time 4 min, time constant 100 ms, modulation amplitude 5 G; microwave power 30 dB; microwave frequency 3.470 (4030 ms), 3.464 (42 ms) GHz, temperature 13 K.

at 4030 ms in Figure 7 to become "smeared" out in the 42-ms spectrum as well as the increase in the overall width of the spectrum.

The S-band EPR linebroadening at 42 ms for mutant **X** (Figure 7, top) can be described only roughly (data not shown) by simulations that use the $^{17}O_{br}$ and $^{17}O_t$ hyperfine tensors determined separately by the ENDOR measurements of samples examined at long times (Table 1), and assuming a site occupancy of $^{17}O_{br}$:$^{17}O_t \approx 1{:}^1/_2$ (recall that, at 42 ms, we estimated that half of the exchangeable label from O_2 has already washed out). Likewise, as shown in Figure 8, the 42-ms ^{17}O ENDOR spectra taken at the fields for the three canonical g values for the Y122F R2 differ in subtle ways from those generated by a similar superposition of $^{17}O_{br}$ and $^{17}O_t$ patterns. With the same assumption about occupancy ($1{:}^1/_2$, $^{17}O_{br}$:$^{17}O_t$), at g values between g_2 and g_3, the 42-ms experimental spectra have additional intensity at higher frequencies (~23 MHz) compared to the simulated spectra.

However, we could jointly simulate the EPR and ENDOR data for mutant **X** quenched at 42 ms by assuming that the diiron center has three discrete conformers (in a ratio 0.2:1:0.2), which differ in the A_3 component of the $^{17}O_{br}$ hyperfine tensor by a total spread of approximately ±30%.[44] The fit to the S-band spectrum is shown in Figure 7, top. This model reproduces the

(44) We also examined a model in which the A_3 component of the $^{17}O_{br}$ hyperfine tensor exhibits a distributed hyperfine strain (distribution of values) at early time. Although optimization of the strain parameters considerably improved the fits of the S-band EPR spectra, the resulting hyperfine parameters did not lead to a satisfactory simulation of the ENDOR data.

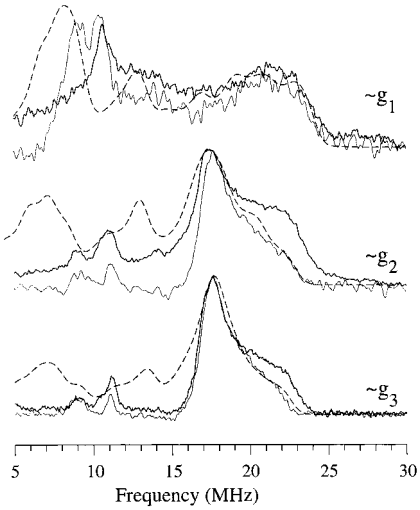

Figure 8. CW ^{17}O ENDOR spectra for **X**($^{17}O_2$) quenched at 42 ms, taken at three different magnetic field positions corresponding to g_1, g_2, and g_3. Black solid line, Y122F mutant protein; thin solid line, wild-type protein; dashed line, superposition of the simulated $^{17}O_{br}$ and $^{17}O_t$ ENDOR patterns as described in text. Experimental conditions: microwave frequency 35.273 GHz (wild-type protein), 35.262 GHz (mutant protein), modulation amplitude 8 G, modulation frequency 100 kHz, rf scan speed 1 MHz/s. The rf frequency has been swept starting at the low-frequency edge. Temperature, 2 K.

ENDOR data equally well (not shown). The parameter set employed for the simulations, however, is not unique. The possibility cannot be excluded that the orientations of the $^{17}O_{br}$ hyperfine and/or quadrupole tensor differ for different conformers. Once these additional parameters are allowed to vary, the number of variables exceeds the number of constraints, and a unique simulation is not feasible.

ENDOR measurements were also performed on **X** prepared with wt R2 and $^{17}O_2$ and quenched at 42 ms. In this case, the properties of $^{17}O_{br}$ and $^{17}O_t$ *are* completely consistent with the properties of these sites in the mutant **X** at long time. As shown in Figure 8, the ENDOR spectra from wt **X** can be well simulated by a superposition of calculated $^{17}O_{br}$ and $^{17}O_t$ patterns obtained using hyperfine tensors determined for the mutant protein at 4030ms, taking their occupancy to be ~$1{:}^1/_2$. The analysis indicates that, at early times, **X** in the Y122F R2 exists in several distinct but similar conformations, and that the structure relaxes over ~10^3 ms to the single conformer that is identical to **X** in the wt R2. The differences seen at early time in the properties of $^{17}O_{br}$ must be quite subtle, because comparisons of the mutant and wt **X** show that ^{14}N, ^1H, and ^{57}Fe data for wt at 42 ms are indistinguishable from those of the mutant at 610 ms (data not shown). These ENDOR results recall the EXAFS finding that the Fe−Fe vector in **X** generated from apo-Y122F R2 had multiple minima, whereas the vector for **X** generated from wt R2 was better defined.[22]

Time Dependence of $^{1,2}H$ Signals. Our earlier work showed that **X** contains an H_xO that is attached to Fe^{III}, while the kinetic studies with $H_2{}^{17}O$ and $^{17}O_2$ suggest that this H_xO is originally derived from O_2 and exchanges with solvent. This leads to a model in which the H_xO is present in **X** at all times, and which thus implies that the proton ENDOR intensity should not vary in time. Therefore, the time-dependent intensities of the proton ENDOR samples were investigated as a function of time, with some of the results shown in Figure 9. At 42-ms quench time, the enzyme shows a ^1H pattern from bound water that is the same in frequencies *and* intensities as that obtained at inter-

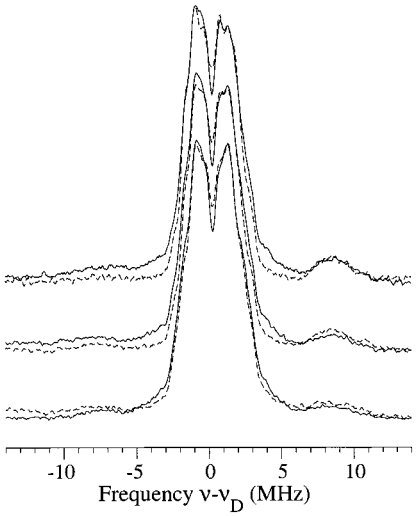

Figure 9. CW proton ENDOR spectra for **X** taken at g_1 (middle spectrum) and fields slightly lower (upper spectrum) and higher (lower spectrum). Quench times: 42 (solid lines) and 4030 ms (dashed lines). Conditions: microwave frequency 35.241 GHz (42-ms quenched sample), 35.174 GHz (4030-ms sample), modulation amplitude 8 G, modulation frequency 100 kHz, rf scan speed 1 MHz/s. The rf frequency has been swept starting at the low-frequency edge. Temperature, 2 K.

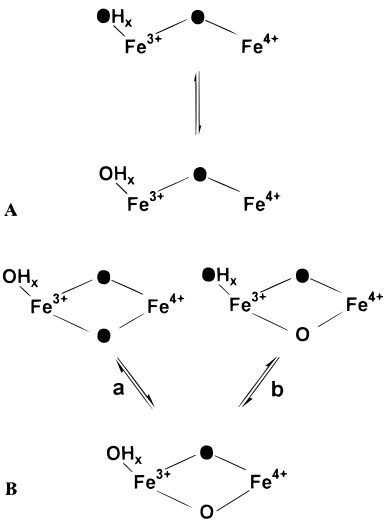

Figure 10. Alternate schemes for the fate of the atoms of O_2 (upper line) in **X** and for the product of exchange with solvent (lower line). Solid oxygens are derived from O_2, and open ones are derived from solvent. Panel A involves a single oxo-bridge, and panel B, two such bridges. In panel B, case a, the two atoms from O_2 initially occur as two μ-oxo bridges; in panel B, case b, initially one atom from O_2 occurs as a bridge and one as a terminal ligand to Fe^{3+}. As discussed in the text, the mono-oxo scheme of panel A is supported by the data.

mediate times and at 4030 ms. These results support our mechanistic model.

Discussion

^{1,2}H ENDOR studies of **X** in H_2O and D_2O buffers led to the proposal that **X** contains the [$(H_xO)Fe^{III}OFe^{IV}$] fragment, with a μ-oxo bridge, a single terminal aqua ligand (water molecule or 2-fold disordered hydroxyl) bound to Fe^{III}, and neither an aqua ligand bound to Fe^{IV} nor an hydroxyl bridge.[21] The strong spin coupling between the iron ions[18] and their short Fe−Fe separation observed by EXAFS spectroscopy[22] require that **X** contains two or three mono-oxo bridges. Our present studies with $^{17}O_2$ and $H_2{}^{17}O$ were carried out to determine the number of oxygenic ligands (two vs three), their source, and their structural arrangement, and thus to further define the total structure of **X**. The results have been complicated *and* enriched by the observation of exchange into **X** of solvent oxygen and exchange out of **X** of O_2-derived oxygen, and by the kinetic complexity of this exchange process.

As described in detail above, the ^{17}O ENDOR studies of **X** prepared in $H_2{}^{17}O$ and with $^{17}O_2$ indicate that **X** quenched at 4 s contains only two types of exogenous oxygenic ligands. At this time, one type (O_t) is completely derived from solvent and is assigned to the single terminal H_xO bound to Fe^{III}. The other type (O_{br}) is assigned to one or more μ-oxo bridges derived from O_2, whose presence is suggested by the strong exchange coupling, the EXAFS data, and the previous resonance Raman experiments.[23] The 42-ms ENDOR experiments carried out in $^{17}O_2$ show that the two atoms of $^{17}O_2$ give rise to one $^{17}O_{br}$ site and one $^{17}O_t$ site. Thus, there can be only a single $^{17}O_{br}$ from $^{17}O_2$. This conclusion is confirmed by the RFQ S-band EPR experiment, which requires that there is but one $^{17}O_{br}$ atom (from gas) at 4 s. As a result, the simplest model consistent with the data is presented in Figure 10A. **X** is formed with one atom of dioxygen as an oxo bridge and the other as a terminal aqua ligand bound to Fe^{III}; the latter oxygen atom exchanges with solvent on the time scale of our experiments, but the former does not.

Could **X** contain a second oxo bridge? In principle, the data do not preclude a di-μ-oxo structure where one bridge is of the O_{br} type and one is of the O_t type, in addition to the terminal aqua ligand. For this proposal to be compatible with the ENDOR data, one would have to postulate that one of the bridging oxygens is of the $^{17}O_{br}$ type, while the properties of the second bridging oxygen and the terminal aqua ligand are identically of the $^{17}O_t$ type, and also that the two O_t sites are exchangeable with solvent. In one scenario, case a of Figure 10B, both oxo bridges are derived initially from O_2, and the terminal oxygen bound to Fe^{III} is derived from solvent. For **X** prepared with $^{17}O_2$, wash-out of the bridging $^{17}O_t$ would leave the single $^{17}O_{br}$ at 4 s; for **X** prepared with $H_2{}^{17}O$, exchange-in would introduce ^{17}O into both of the presumedly equivalent O_t sites, one as H_xO and one as an oxo bridge. Alternatively, one might consider case b of Figure 10B, with one oxygen from $^{17}O_2$ becoming a μ-oxo bridge and the second H_xO, while the second μ-oxo bridge comes from solvent. Again, ENDOR of **X** in $H_2{}^{17}O$ at 4 s would require the coordinated H_xO and the second μ-oxo bridge to have identical ENDOR spectra. However, we believe that it is not possible for two such chemically different sites, a terminal water/hydroxo and a bridging oxo, to have *identical* ENDOR parameters. Thus, the ability to precisely simulate the ENDOR spectra of **X** generated in $H_2{}^{17}O$ and $^{17}O_2$ at 4 s suggests that a di-μ-oxo bridge structure for **X** is highly unlikely.[45]

There remains the question not addressed by ENDOR as to the number and nature of the carboxylato bridges between the two iron ions of **X**, as indicated in Figure 11. The short Fe−Fe distance observed by EXAFS methods appears to require one and possibly mono-oxo bridges in addition to the single oxo-bridge, which could be derived from either E115 or E238, or both.[22]

*We thus conclude that the fate of dioxygen during the formation of **X** is represented by Figure 10A, and further suggest that **X** has structure b of Figure 11.*

(45) In principle, ^{17}O linebroadening measurements could confirm our conclusion that **X** at 4 s contains one, not two, O_t sites, but the effects are not reliably measurable with the low-enrichment (35%) $H_2{}^{17}O$ available, and indeed simulations show that enrichments of no less than 70% would be required.

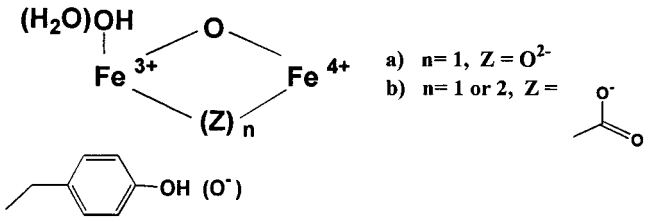

Figure 11. Alternative structures for **X**. To maintain charge neutrality of the site, if the terminal ligand to Fe^{3+} is (OH^-), then the tyrosine is protonated; if the terminal ligand is H_2O, then tyrosine is deprotonated.

What remains puzzling is the kinetics of wash-in/wash-out of the water bound to Fe^{III} of the **X** cluster. Both the ENDOR and S-band EPR studies at 42 ms in comparison with those at 4 s suggest that 50% of the label in H_2O derived from O_2 has already exchanged. Over the next 4 s, the remainder of the O_2 derived H_2O washes out, indicating at a minimum, biphasic kinetics for wash-out. At present we do not understand the mechanistic basis for this observation. Two interpretations of the biphasic kinetics are being considered. First, it is possible that the exchange observed at 42 ms has occurred from a precursor to **X**. It is chemically unlikely that such an exchange could occur from any peroxo precursor, and thus this interpretation implies the existence of an intermediate between the putative peroxo and **X**. A second possible interpretation relates to the observation for all R2s that have been examined, that some of the diferric clusters form without the concomitant oxidation of Y122 to the tyrosyl radical. It has not been established whether **X**, which is the precursor to the diferric clusters adjacent to a ·Y122, is also the precursor to those adjacent to a reduced tyrosyl residue, or whether in the latter case the diferric cluster is formed by a different mechanism. One might speculate that both types of diferric cluster are formed from **X** and that the two phases of the exchange are associated with the two types of center. However, this appears not to be so because many experiments with both wt R2 and Y122F R2 show that the maximum amount of **X** observed (1.0−1.2 equiv per equivalent of R2) is the same, within experimental error, as the amount of ·Y122 that is formed (∼1.2 equiv). Thus, if **X** does exhibit biphasic kinetics because there are two protein forms, then the **X** in both forms oxidizes the tyrosine. To us this is an argument for the interpretation in which exchange occurs in a precursor to X.

The ^{17}O ENDOR experiments have thus allowed us to further refine the structure of **X.** One remaining question is whether Fe^{IV} or Fe^{III} is closest to Y122. It has recently been proposed, on the basis of a Mössbauer time course of the assembly process and a structure of mouse R2 at pH 4.7 that contains a single iron, that Fe^{III} is adjacent to Y122.[46,47] While thought-provoking, this assignment is based on a structure of an inactive protein in which the protonation state of the carboxylates within the active site could modulate metal occupancy. As the location of each iron relative to Y122 is a key to further definition of the structure of X, we are using *m*-F-tyrosine-labeled R2 and ^{19}F ENDOR experiments to further address this assignment. A second structural question relates to the protonation state of Y122 in the presence of **X** (Figure 10). One proposal is that the proton of Y122 has been transferred to generate the H_2O bound to Fe^{III} during the formation of **X**. The resulting tyrosinate would then be easier to oxidize to ·Y122 in the subsequent step of the assembly process. Alternatively, if **X** contains an Fe^{III}-bound hydroxide and is adjacent to protonated Y122, the hydroxide could assist in its deprotonation, facilitating electron transfer. Proton release experiments under single turnover conditions are in progress to distinguish these two possibilities from others.

Acknowledgment. The authors express their gratitude to C. E. Davoust for his technical support, to Drs. P. E. Doan, H.-I. Lee, and D. Tierney for helpful discussions, and especially to Dr. J. A. Telser for programming the DDPOWHE simulation program. This work has been supported by the NIH (HL13531, B.M.H.; GM29595, J.S.) and by the NSF (MCB 9507061, B.M.H.)

JA9824270

(46) Bollinger, J. M. Jr.; Chen, S.; Parkin, S. E.; Mangravite, D. E.; Ley, B. A.; Edmondson, D. E.; Huynh, B. H. *J. Am. Chem. Soc.* **1997**, *119*, 5976−5977.

(47) Kauppi, B.; Nielsen, B. B.; Ramaswamy, S.; Larsen, I. K.; Thelander, M.; Thelander, L.; Eklund, H. *J. Mol. Biol.* **1996**, *262*, 706−720.